Journal of Structural Geology 33 (2011) 329–342

Contents lists available at ScienceDirect

Journal of Structural Geology

journal homepage: www.elsevier.com/locate/jsg

Himalayan hinterland-verging superstructure folds related to foreland-directed infrastructure ductile flow: Insights from centrifuge analogue modelling

Laurent Godin [a,*], Chris Yakymchuk [a], Lyal B. Harris [b]

[a] Department of Geological Sciences and Geological Engineering, Queen's University, Kingston, Ontario K7L 3N6, Canada
[b] Institut national de la recherche scientifique, centre - Eau Terre Environnement, 490 de la Couronne, Quebec City, Quebec G1K 9A9, Canada

ARTICLE INFO

Article history:
Received 3 January 2010
Received in revised form
29 August 2010
Accepted 13 September 2010
Available online 4 November 2010

Keywords:
Centrifuge analogue modelling
Channel flow
Himalaya
Tectonics
Detachment shear zones

ABSTRACT

The orogenic superstructure (SS) and infrastructure (IS) constitute two levels of a mountain belt with contrasting structural styles. In the Nepal Himalaya, N-verging back folds, which oppose the orogenic vergence, dominate the SS. Competing explanations for these folds are tested using centrifuge analogue models. Modelling suggests that SS folding occurs during bulk shortening accompanied by IS thickening before IS flow. Focused erosion then instigates IS lateral flow and stretching, decoupling of the SS, and transposition of the lower SS into a detachment zone. Decoupling at the IS–SS interface separates an SS dominated by older folds and an IS characterised by younger horizontal transposition and stretching of early folds. Extrusive ductile flow of the IS locally modifies fold vergence in the SS. The fold asymmetry is thus controlled by the efficiency of coupling between IS and SS; a low viscosity at the IS–SS interface favours complete decoupling and hinders modification of fold vergence, whereas a higher viscosity IS-SS interface favours fold vergence modification. Modelling supports a tectonic scenario in which Himalayan hinterland-verging folds are the product of early shortening of the SS followed by local modification of fold geometry when the IS subsequently stretches and flows during focused erosion and melt-enhanced IS weakening.

1. Introduction

Continental crust undergoing regional deformation displays complex vertical strain distribution (or zonation) reflecting dominant deformation processes that vary with depth. The superstructure is typically characterised by upright folds in low metamorphic-grade rocks, indicative of bulk horizontal shortening, whereas the subjacent infrastructure contains high-metamorphic grade migmatitic rocks with gently-inclined, strongly-transposed features emblematic of horizontal stretching and shearing (Wegmann, 1935). The terms "superstructure" and "infrastructure" are used here to describe crustal-scale differences between the upper crust, which dominantly deforms by frictional-plastic (Coulomb-type) failure, and the underlying mid-crust in which the deformation is dominated by power-law creep. The superstructure-infrastructure classification has recently been revived in the literature, partly due to its similarities with and applicability to numerical models of continental collision that produce mid- to lower crustal flow (Beaumont et al., 2001, 2006; Culshaw et al., 2006). In such models, the weakened mid-crust responds either to the introduction of a lower crustal indenter (Culshaw et al., 2006), or an imposed lithostatic pressure gradient by flowing laterally towards the orogenic front beneath a comparatively passive orogenic superstructure (Beaumont et al., 2001, 2006; Godin et al., 2006a, for review).

In this paper, analogue centrifuge models are used to investigate contrasting deformation styles in the superstructure and infrastructure observed in continental collision zones. Models are designed to simulate the structural evolution of horizontal shortening in a superstructure/infrastructure package, followed by vertical thinning and horizontal stretching and ductile flow of the melt-weakened infrastructure due to focused erosion and a lithostatic pressure gradient in a manner akin to channel flow. Emphasis in this study is placed on examining: (1) coeval and dynamically linked deformation (coupling) between the superstructure and infrastructure; (2) the formation of drag folds along the interface between the superstructure and infrastructure during infrastructure horizontal flow; and (3) the effects of varying the slope steepness of the orogenic topographic front, which drives extrusion of the ductile infrastructure, on the development of deformation features in the superstructure. Specifically, centrifuge analogue modelling is used to test whether hinterland-verging folds can develop above a sub-horizontally stretching foreland-directed ductile-flowing infrastructure (e.g. Larson et al., 2010).

* Corresponding author. Fax: +1 613 533 6592.
E-mail address: godin@geol.queensu.ca (L. Godin).

0191-8141/$ – see front matter © 2010 Elsevier Ltd. All rights reserved.
doi:10.1016/j.jsg.2010.09.005

Our modelling approach, in particular, investigates hinterland-directed folds preserved in the Tethyan sedimentary sequence, the Himalayan superstructure in central Nepal, where anomalous north-verging folds of unresolved age dominate (Bordet et al., 1971; Godin et al., 1999a; Godin, 2003; Kellett and Godin, 2009). These folds are preserved in the hanging wall of a crustal-scale detachment, the South Tibetan detachment system (STDS), below which the infrastructure, the Greater Himalayan sequence, has been extensively transposed and metamorphosed (Fig. 1; Grujic et al., 1996; Vannay and Hodges, 1996; Grasemann et al., 1999; Searle and Szulc, 2005; Jessup et al., 2006; Larson and Godin, 2009).

2. The superstructure-infrastructure association and the Himalayan orogen

2.1. The superstructure-infrastructure concept

A common observation in orogenic belts is the change in dominant structural style from upright open folds in the superstructure to isoclinal recumbent folds in the infrastructure (Murphy, 1987; Godin, 2003; Williams and Jiang, 2005; Culshaw et al., 2006; Williams et al., 2006; Denèle et al., 2009; Kellett and Godin, 2009). In this paper, the superstructure of an orogenic belt refers to the weakly metamorphosed to unmetamorphosed sedimentary sequence resting on the underlying migmatitic infrastructure. The rheology of the superstructure renders it mostly susceptible to brittle and brittle-ductile deformation. A crustal-scale detachment, usually marked by a strain gradient across which rheology and structural styles are often contrasting, separates the infrastructure from the superstructure. The infrastructure refers to the ductile, thermally-weakened middle-crust that is of a similar density and lesser viscosity than the overlying superstructure (Mecklenburgh and Rutter, 2003; Rosenberg and Handy, 2005). Examples of such infrastructure–superstructure relationships are found in several orogens, such as the Canadian Cordillera (Murphy, 1987; Glombick et al., 2006), the Western Superior Province of Canada (Culshaw et al., 2006), the French Pyrenees (Denèle et al., 2009), the Oman ophiolitic belt (Searle et al., 2004), and the Australian Petermann orogen (Raimondo et al., 2009).

2.2. The Himalayan prototype

The Himalayan orogen is the type example of a large hot orogen, characterised by a viscous mid-crust that contains significant *in situ* partial melts and where the channel flow process may have been operative (Bird, 1991; Grujic et al., 1996, 2002; Royden et al., 1997; Clark and Royden, 2000; Beaumont et al., 2001, 2006).

The Himalayan orogen initiated in early Eocene times, following collision of the Indian and Eurasian plates (see Hodges, 2000 and Yin and Harrison, 2000 for reviews). The convergence culminated in closure of the Tethyan Ocean, southward imbrication of the Indian crust, and northward continental subduction of Indian lower crust and lithospheric mantle beneath Asia (Hodges, 2000; Yin and Harrison, 2000). The Himalayan orogen consists of five, broadly parallel lithotectonic belts, separated by mostly north-dipping faults. The Greater Himalayan sequence is bounded by two parallel and opposite-sense shear zones that were both broadly active during the Miocene (Fig. 1; Hubbard and Harrison, 1989; Searle and Rex, 1989; Hodges et al., 1992, 1996; chronological review in Godin et al., 2006a). The Main Central thrust (MCT) zone marks the lower boundary of the Greater Himalayan sequence, juxtaposing the metamorphic core above the underlying Lesser Himalayan sequence (Searle et al., 2008). The STDS defines the upper boundary roof fault of the Greater Himalayan sequence, placing it in tectonic contact with the overlying weakly- to unmetamorphosed Tethyan sedimentary sequence (Burg and Chen, 1984; Burchfiel et al., 1992; Searle and Godin, 2003).

The apparent coeval movement of the MCT and STDS, combined with the presence of highly sheared rocks and high grade to migmatitic rocks within the Greater Himalayan sequence, has led many workers to view the metamorphic core as a north-dipping, southward extruding slab of mid-crustal material flowing away from the thick southern edge of the Tibetan Plateau, towards the thinner foreland fold-thrust belt (Grujic et al., 1996, 2002; Law et al., 2004; Searle and Szulc, 2005; Jessup et al., 2006; Godin et al., 2006a; Cottle et al., 2007; Larson and Godin, 2009; Larson et al., 2010).

2.2.1. The Himalayan infrastructure: The Greater Himalayan sequence

The Greater Himalayan sequence, where exposed at the surface, comprises greenschist to granulite facies metamorphic rocks. The structural upper half of the Greater Himalayan sequence is dominated by migmatites and discontinuous Miocene leucogranite bodies (Fig. 2). The Greater Himalayan sequence is pervasively transposed by top-to-the-south shear fabrics (Mattauer, 1975; Grujic et al., 1996; Grasemann et al., 1999; Jessup et al., 2006; Larson and Godin, 2009). Microstructural analysis and metamorphic studies indicate that these ductile fabrics developed at peak temperatures at ca. 21 Ma, coincident with southward extrusion (Daniel et al., 2003; Hollister and Grijuc, 2006; Larson and Godin, 2009; Larson et al., 2010). Vorticity studies yield kinematic vorticity numbers between 0.49 and 0.80 (66% to 41% pure shear), with a significant amount of stretch (34–47%) parallel to the flow plane (Grasemann et al., 1999; Law et al., 2004; Jessup et al.,

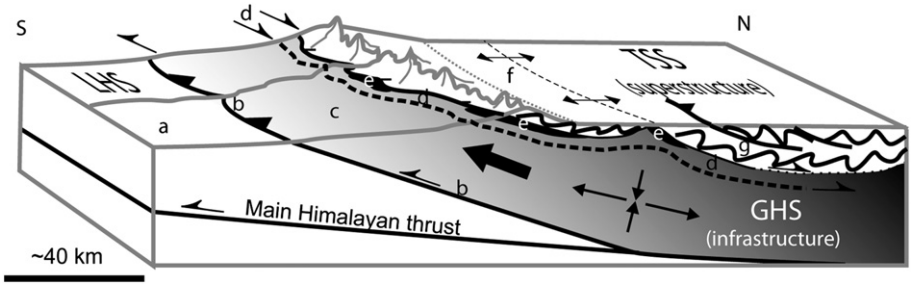

Fig. 1. Sketch depicting the Himalayan infrastructure and north (hinterland)-verging folds within the superstructure. The small half arrows indicate the hanging wall sense of displacement on faults. The small black arrows depict the state of non-coaxial general shear preserved in the Himalayan infrastructure (e.g. Larson and Godin, 2009 and references therein). The thick black arrow portrays the direction of extrusion of the infrastructure during synchronous motion of its bounding faults; (a) lesser Himalayan sequence (LHS), (b) main Central thrust, (c) Greater Himalayan sequence (GHS), (d) South Tibetan detachment system, (e) Miocene leucogranites, (f) Tethyan sedimentary sequence (TSS), (g) north-verging folds, which are localised in the immediate hanging wall of the South Tibetan detachment system in central Nepal (Godin, 2003; Kellett and Godin, 2009).

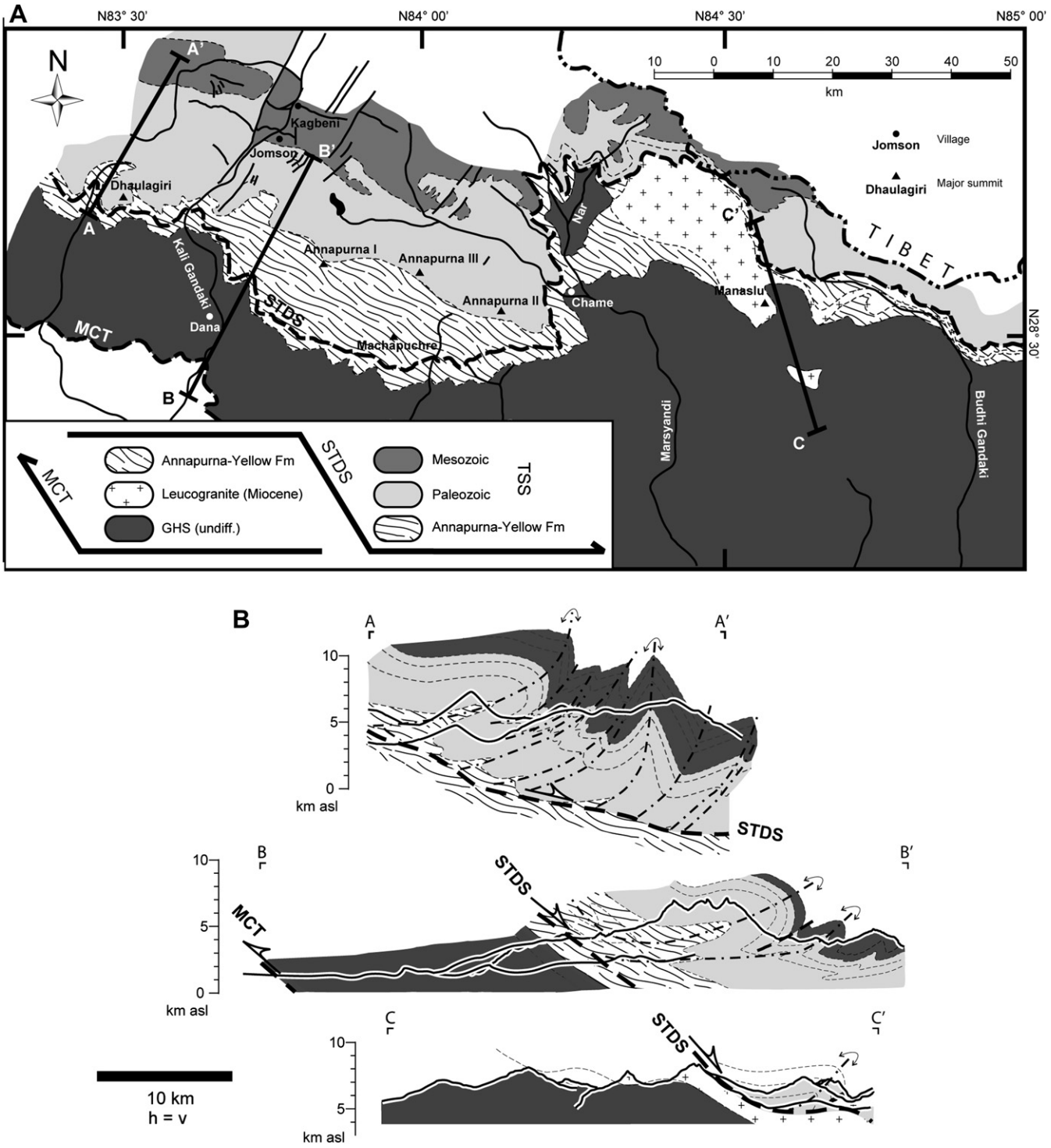

Fig. 2. (A) Geological map of central Nepal (modified from Colchen et al., 1981; Godin, 2003; Searle et al., 2008; Larson and Godin, 2009; Larson et al., 2010). (B) Cross sections displaying north-verging folds preserved in the Tethyan sedimentary sequence (TSS), above the South Tibetan detachment system (STDS) and highly-strained Greater Himalayan sequence (GHS). MCT, Main Central thrust. Section A–A′: Kellett and Godin, 2009; Section B–B′: Godin, 2003; Section C–C′: modified from Larson et al. (2010).

2006; Carosi et al., 2006, 2007; Larson and Godin, 2009; Larson et al., 2010). This suggests that the Greater Himalayan sequence deformed by a combination of vertical thinning and horizontal stretching (Larson and Godin, 2009; Larson et al., 2010). The uppermost ~1 km portion of the Greater Himalayan sequence is characterised by a kinematic reversal in shear-sense that defines the top-to-the-north-sense STDS (Burchfiel et al., 1992; Searle and Godin, 2003).

In central Nepal, the Greater Himalayan sequence records two Cenozoic thermal pulses associated with Himalayan orogenesis: (1) Eocene–Oligocene burial metamorphism at ca. 35 Ma, and (2) Miocene peak temperature metamorphism at ca. 21 Ma, coeval with mid-crustal ductile flow (Hodges, 2000). Structural and $^{40}Ar/^{39}Ar$ thermochronological data suggest that ductile flow and southward extrusion of the Greater Himalayan sequence terminated with cessation of movement on the brittle upper strand of

the STDS at ~19 Ma, which was followed almost immediately by hinterland-directed out-of-sequence deformation and rapid exhumation, and by activation of new thrusts structurally below the Greater Himalayan sequence (Godin et al., 2006b; Robinson et al., 2006; Larson et al., 2010).

2.2.2. The Himalayan superstructure: the Tethyan sedimentary sequence

The Tethyan sedimentary sequence forms the superstructure to the Greater Himalayan sequence (Fig. 2). In the central Nepal Himalaya, the Tethyan sedimentary sequence is a ca. 12 km thick unmetamorphosed to weakly metamorphosed Palaeozoic and Mesozoic sedimentary sequence, which was deposited on the northern Indian palaeocontinental margin and subsequently deformed during Himalayan orogenesis (Fig. 2b; see Garzanti, 1999 for complete stratigraphic framework).

In central Nepal, the Palaeozoic section is characterised by massive limestone, calcareous shale and pelite, with local dolomitic and quartzitic horizons (Fig. 2a; Bordet et al., 1971; Colchen et al., 1981; Garzanti, 1999). The Mesozoic stratigraphy comprises calcareous shale, grading upwards to limestone and black shale, which are capped by clastic units (Bordet et al., 1971; Gradstein et al., 1992).

The Tethyan sedimentary sequence has been subjected to polyphase deformation, yet is structurally dominated by north-verging back folds whose asymmetry is opposite to the orogenic vergence (Fig. 2b; Godin et al., 1999a; Godin, 2003). The absolute age of these folds is uncertain, although cross-cutting relationships indicate that they predate the dominant Miocene motion along the STDS at ~21 Ma (Guillot et al., 1993; Godin et al., 1999a, 2001; Kellett and Godin, 2009). Palinspastic bed length restoration of the north-verging folds implies a minimum 35% shortening, and a minimum 150% vertical thickening (Godin, 2003; Kellett and Godin, 2009). These data suggest that north-verging folds played a significant role in pre-Miocene crustal thickening (150–180% thickening of 12 km stratigraphy = approximately 20-km thick) of the Himalayan superstructure, possibly predating or coinciding with Eocene–Oligocene burial metamorphism (ca. 35 Ma) preserved in the underlying Greater Himalayan sequence (Godin et al., 1999a, 2001; Aikman et al., 2008).

2.2.3. Models for Himalayan superstructure hinterland-directed deformation

Competing models have been proposed to explain the presence of hinterland-verging folds in the Tethyan sedimentary sequence of central Nepal. Early work suggested that the folds were formed by gravity-induced sliding and drag folding coeval with motion along the STDS (Fig. 3a; Bordet et al., 1971; Colchen et al., 1981; Burg and Chen, 1984; Burchfiel and Royden, 1985; Burchfiel et al., 1992). Others proposed that the north-verging folds represent features related to an early compression and crustal-thickening event that occurred prior to Miocene displacement along the STDS (Fig. 3b; Godin et al., 1999a, 2001). Alternatively, it has been suggested that the north-verging folds may have developed while the STDS was the active upper boundary of southward-extruding Greater Himalayan sequence rocks; the folds recording the opposite shear drag folding effect of a flowing mid-crustal channel (Fig. 3c; Carosi et al., 2007). More recently, Kellett and Godin (2009) argued that drag owing to the southward transport of the mid-crustal Greater Himalayan sequence may have modified the geometry of already existing folds, causing the northward vergence of the folds in the Tethyan sedimentary sequence (Fig. 3d). Previous attempts to link superstructural features with infrastructural thermal events (e.g. Godin et al., 1999a, 2001; Kellett and Godin, 2009) have been hindered by a lack of absolute ages for shortening features in the Tethyan sedimentary sequence.

The centrifuge modelling approach described in the following section therefore provides a means to test the geometric, kinematic, and dynamic feasibility of these competing folding models for the Himalayan superstructure and possible genetic links with underlying ductile flow of the infrastructure.

3. Experimental approach

Analogue materials with properties scaled to represent both the layered Tethyan sedimentary sequence (the superstructure) and the underlying low-viscosity Greater Himalayan sequence (the infrastructure) were used (Tables 1 and 2). The models are deformed in a high-acceleration centrifuge to trigger infrastructural horizontal stretching ductile flow. The main goals of experiments are to produce superstructural hinterland-verging folds by either:

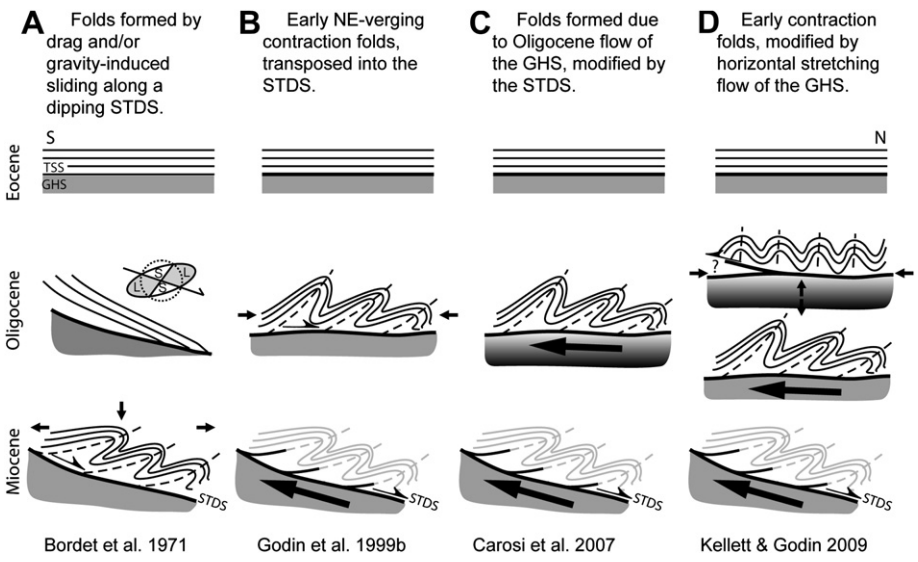

Fig. 3. End-member models for the formation of back-folds, modified from Kellett and Godin (2009). Light grey is used to indicate deformation that is no longer occurring. Black indicates active deformation. The darkening gradient portrayed in C and D represents the thermally-weakened middle crust implied in these models. TSS, Tethyan sedimentary sequence; GHS, Greater Himalayan sequence; STDS, South Tibetan detachment system; S and L (in A) denote the shortening and lengthening quadrants of the strain ellipse, respectively.

Table 1
Scaling properties of models and prototype.

Quantity	Model	Prototype	Scaling ratio
Length ratio	1 mm	1 km	$l_r = l_m/l_p = 1 \times 10^{-6}$
Density (bulk) (kg m^{-3})			
Superstructure	1050[a]	2700	$\rho_r = \rho_m/\rho_p = 0.39$
Infrastructure	1050[a]	2700	$\rho_r = \rho_m/\rho_p = 0.39$
Acceleration	1000	1	$a_r = 1000$
Velocity (mm yr^{-1})	2.3×10^{6}[b]	59	$v_r = l_r/t_r = 3.98 \times 10^{4}$
Time	360 s[c]	0.44 my[b]	$t_r = \mu_r/l_r\rho_r$, $a_r = 2.6 \times 10^{-11}$
Viscosity (Pa s)			
Superstructure	1×10^{7}[d]	1×10^{21}	$\mu_r = \mu_m/\mu_p = 1 \times 10^{-14}$
Infrastructure	1×10^{5}[d]	1×10^{19}[e]	$\mu_r = \mu_m/\mu_p = 1 \times 10^{-14}$

[a] Density varies with the proportion of the different materials in any given sample. On average, both levels are approximately 1050 kg m^{-3}. The superstructure ranges from ~990 to 1100 kg m^{-3}, and the infrastructure ranges from ~1010 to 1070 kg m^{-3}. Densities were calculated with a Grabner Instruments Minidens solids densitometer with reproducibility of ±10 kg m^{-3} (~1%).
[b] Calculated for 25 mm shortening each run.
[c] Run-up/down times are not taken into consideration for scaling.
[d] Approximate effective viscosity at experimental strain rates of ca. 5×10^{-4} s^{-1}.
[e] Channel flow requires 1×10^{19} Pa s in thermo-mechanical models (Jamieson et al., 2004; Beaumont et al., 2006), but this value is probably lower in nature (Mecklenburgh and Rutter, 2003; Rosenberg and Handy, 2005).

(1) horizontal infrastructural flow alone, or (2) modifying the vergence of already established folds by triggering infrastructural horizontal flow during the evolution of the system. Finally, various angles of the foreland topographic front are used to obtain insight on the efficiency of erosion in driving extrusion of the infrastructure.

3.1. Centrifuge apparatus

A high-acceleration centrifuge is used to dynamically scale gravitational forces deemed important to the evolution of orogen-scale structures, especially those developed during channel flow (Beaumont et al., 2001, 2006; Godin et al., 2006a). The PR-7000 centrifuge at the Institut National de la Recherche Scientifique in Quebec City is capable of subjecting models up to 200 mm x 80 mm in plan view to accelerations exceeding 1000 *g* (where *g* is the local acceleration due to gravity). For a detailed explanation of the centrifuge method, readers are referred to Ramberg (1981) and Dixon and Summers (1985). Models were run in 6–8 stages, each for 360 s at 900 *g* with a run-up time of 60 s and a run-down time of 420 s. In between each stage, vertical sections through the models parallel to the shortening direction were cut at intervals of ~5 mm from both ends to be photographed.

3.2. Initial model geometry, materials, and scaling

Initial model dimensions are 170 mm × 80 mm in plan view by 20–30 mm in height (Fig. 4a). Where applicable, models were shortened via a collapsing wedge 30 mm × 80 mm in plan view by 50 mm in height that is placed at the hinterland to induce layer-parallel shortening based on the method of Dixon and Tirrul (1991). A weighted plastic plate is inserted between the model and the collapsing wedge to provide an equal distribution of force throughout the hinterland face of the model (Johns and Mosher, 1996). Models consist of a ~10-mm thick brittle-ductile superstructure overlying a ductile ~5-mm thick infrastructure (Fig. 4b; Table 2). Individual models have slight lateral variations in layer thickness within the superstructure; however, the dynamic effect of this, with respect to behaviour of the entire superstructure, is interpreted to be minimal.

Model materials are consistent with materials utilised in published centrifuge studies that simulate different levels of the crust where material properties and scaling have been previously discussed (Dixon and Summers, 1985; Dixon and Tirrul, 1991; Koyi, 1991; Koyi and Skelton, 2001; Harris and Koyi, 2003; Corti, 2004). The superstructure is represented by microlaminates composed of Demco® modelling clay, Dow Corning 3179 dilatant compound (a silicone bouncing putty), and Crayola Model Magic® (a low density modelling clay), analogous to a succession of competent clastics, carbonates and incompetent pelitic and semi-pelitic units (Dixon and Tirrul, 1991) and similar to the stratigraphy of the Tethyan sedimentary sequence (Garzanti, 1999). A thin layer of low-density Crayola Model Magic® modelling clay is placed at the surface to

Table 2
Model composition.

Model/Level	Material	Thickness (mm)	
Model 47			
Cap	White Crayola Model Magic[a]	4	
Superstructure		7	
	Dow Corning Dilatant compound 3179	0.146	
	Microlaminates of Blue Demco with 40 % Crayola Model Magic	0.146	Package repeated 16 times
	Blue Demco with 10% Crayola Model Magic	0.146	
Infrastructure	Layered yellow and red Crazy Aaron with a discontinuous green basal layer	4	
Model 50			
Cap	White Crayola Model Magic	5	
Superstructure		10	
	Brown Demco	0.031	
	Blue Demco and 40% Crayola Model Magic	0.208	Package repeated 16 times
	Orange Demco and 40% Crayola Model Magic	0.312	
Infrastructure	Layer of Polydimethylsiloxane (half the model)	0.5	
	Layered yellow and green Crazy Aaron putty	6	
Model 43			
Cap	White Crayola Model Magic	4	
Superstructure		8	
	Blue Demo mixed with 10% crayola Model Magic	0.1	
	Blue Demco	005	
	Dow Corning Dilatant compound 3179	0.5	Package repeated 8 times
	Brown Demco mixed with 40% Crayola Model Magic	0.35	
Infrastructure	Interlayers of yellow, red, and yellow Crazy Aaron with a discontinuous basal green layer	7	

[a] This layer caps all models to maintain the structural integrity during deformation and is used instead of a layer simulating upper brittle crust.

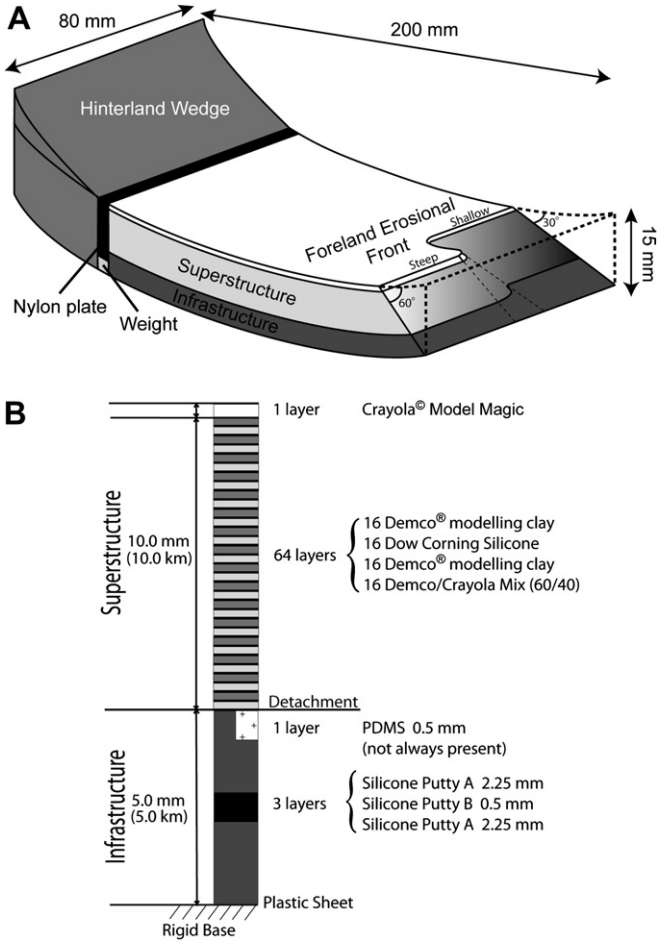

Fig. 4. (A) Model set-up showing the collapsing wedge in the hinterland that activates layer-parallel shortening, similar to Dixon and Tirrul (1991). Models consist of a 10 mm thick brittle–ductile superstructure overlying a 5 mm thick ductile infrastructure. A weighted nylon plate is inserted between the model and the collapsing wedge to provide an equal distribution of force across the hinterland face of the model. The portrayed irregular erosion front was created on some models, while others contained an extra layer of polydimethylsiloxane (PDMS), a clear, low density and viscosity polymer, at the infrastructure-superstructure interface. (B) Model composition. Note that a thin (0.5 mm) layer of PDMS was introduced in some models to mimic the presence of migmatites and leucogranites in the immediate footwall of the South Tibetan detachment system. All models were covered by a thin layer (1–2 mm) of low-density Crayola Model Magic.

buffer the density contrast between the uppermost superstructure and air (Fig. 4) as no brittle, upper crustal layer was included. The infrastructure of the models is composed of Crazy Aaron Enterprises Thinking Putty®, a silicone putty (similar to Dow Corning Rhodorsil Gomme® whose composition and properties are described by Weijermars, 1986) with scaled densities and viscosities that represent ductile melt-weakened mid-crust. Effective viscosities of materials at experimental strain rates are presented in Fig. 5. In the models, the ductile infrastructure has approximately the same density (<2% difference; Table 1) as the superstructure, although in reality the weakened infrastructure may be slightly less dense, proportional to the quantity of *in-situ* partial melt (Rosenberg and Handy, 2005). Putties of different colours that exhibit minimal dynamic variation are interlayered for visual contrast (Fig. 4b). The formation of bubbles during layer construction was unavoidable and minor bubbles are noted in centrifuge experiments using layered materials (e.g. Koyi, 1991; Johns and Mosher, 1996; Harris and Koyi, 2003; Koyi and Skelton, 2001). Bubbles and irregularities in the surface of the microlaminates act as minor heterogeneities that help

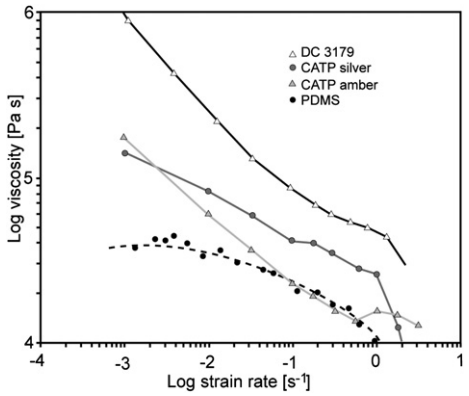

Fig. 5. Compilation of flow properties of Dow Corning 3179 dilatant compound (DC 3179; Poulin, 2006), Crazy Aaron Thinking Putty (CATP; Poulin, 2006), and polydimethylsiloxane (PDMS; Weijermars, 1986; ten Grotenhuis et al., 2002).

nucleate folds (as noted by Johns and Mosher, 1996); indeed such irregularities are important in simulating natural rock deformation where perturbations are commonly required for folds to nucleate and greatly influence the resulting fold style (e.g. Brun and Merle, 1988; Williams and Jiang, 2001; Alsop et al., 2007) and have been introduced in numerical models of folding (e.g. Mancktelow, 1999). Scaling parameters are summarised in Table 1. Scaling laws of Hubbert (1937) and Ramberg (1967, 1981) are used to construct dynamically and geometrically scaled models; scaling parameters are similar to those of models by Koyi (1991). Model geometry is based on the central Nepal Himalaya with the Tethyan sedimentary sequence representing the superstructure and the Greater Himalayan sequence representing the infrastructure, as described in the previous section. Length is scaled such that 1 mm in the model equates to 1 km in the natural prototype.

In numerical models and nature, the infrastructure is rheologically similar to the superstructure in the early stage of orogenesis and only after a period of thermal incubation does the infrastructure sufficiently weaken (Jamieson et al., 1998, 2004). However, limitations in modelling materials and apparatus require the use of a ductile infrastructure at the onset of orogenesis. This constraint is accommodated by the lack of erosion during the shortening phase, which inhibits lateral ductile flow of the infrastructure until later erosion initiates it. Average slope angles for central Nepal are 30° (Gabet et al., 2004) and in some areas of the Himalaya can be up to 60° (Burbank et al., 1996). Length limitations of the modelling apparatus does not permit a frontal hillslope angle less than 30°, whereas a hillslope angle greater than 60° is unrealistic; therefore, 30° and 60° are selected to represent average and extreme hillslope angles, respectively. It is important to emphasize that the erosion front angles are mainly imposed on the models to promote lateral flow of the infrastructure, not to precisely scale the Himalayan hillslope front.

An additional limitation to the modelling apparatus is the inability with the current setup to replenish the infrastructure as it flows out of the model through the frontal erosional front. Broad superstructure synforms may partly pinch-out the infrastructure, in turn instigating minor hinterland-directed infrastructure flow. Consequently, the geometry of the last stage of the models must be taken with a note of caution.

4. Results

Modelling investigates the influence of three parameters on the ability to produce back-verging folds in the model superstructure: (1) amount and sequence of shortening required to instigate drag

folding; (2) presence or absence of less-viscous ductile layer at the detachment; and (3) angle of focused erosion front.

4.1. Erosion and infrastructure flow below an unfolded layered superstructure

The goal of this experiment was to evaluate if underlying horizontal ductile stretching flow (stretching in the direction of flow) of the infrastructure could create superstructural folds, as suggested by Carosi et al. (2007) (Fig. 3c). Model 47 (95 mm length) consists of an undeformed layered superstructure resting above a homogeneous infrastructure (Table 2).

An erosion front was cut at the foreland-end of the model before the initial run. This was done to impose at the onset a lateral lithostatic pressure gradient deemed essential for mid-crustal flow (i.e. channel flow; Beaumont et al., 2001). The erosion front was cut right down to the base of the infrastructure, with half the model having a steep ~60°–80° front and the other half with a shallow ~30°–45° front (and a gentle curved transition between the two erosion fronts – see Fig. 4). The model was run in seven stages; the erosion front angle was re-cut after each step to maintain initial configuration. The last two stages of this experiment were run at peak acceleration (~1100 *g*) for 15 min with the same run-up and a slightly longer run-down time in an attempt to trigger superstructural folding.

The model behaved similarly with a steep or shallow erosion front. No deformation was recorded in the superstructure in either case, whereas significant horizontal stretching and vertical thinning occurred in the infrastructure (Fig. 6). The superstructure microlaminates remain parallel and were not affected by either flow-parallel extension or shortening. Although a single erosion front was maintained, the infrastructure unexpectedly flowed towards the erosion front and the rigid backstop. Despite the fact that the model did not behave as originally envisaged, the results show that at no time during the experiment can the infrastructural horizontal flow trigger superstructure folding.

4.2. Infrastructural flow below already established superstructure folds – the influence of detachment ductility

The second experiment (Model 50) was run to assess the influence of the ductility of the detachment on the potential for superstructural fold geometry modification (Fig. 7). In this model, a 0.5-mm thick layer of Polydimethylsiloxane (PDMS), simulating migmatites and melt pooling in the upper part of the infrastructure, is incorporated on half the superstructure-infrastructure interface to investigate its effects on superstructure fold geometry and superstructure-infrastructure decoupling efficiency (Table 2).

The model underwent two stages of shortening without erosion (31% of total shortening), followed by four stages during which the erosion front was created and then maintained at 40° dip (Fig. 7). The erosion front was cut down to the base of the infrastructure.

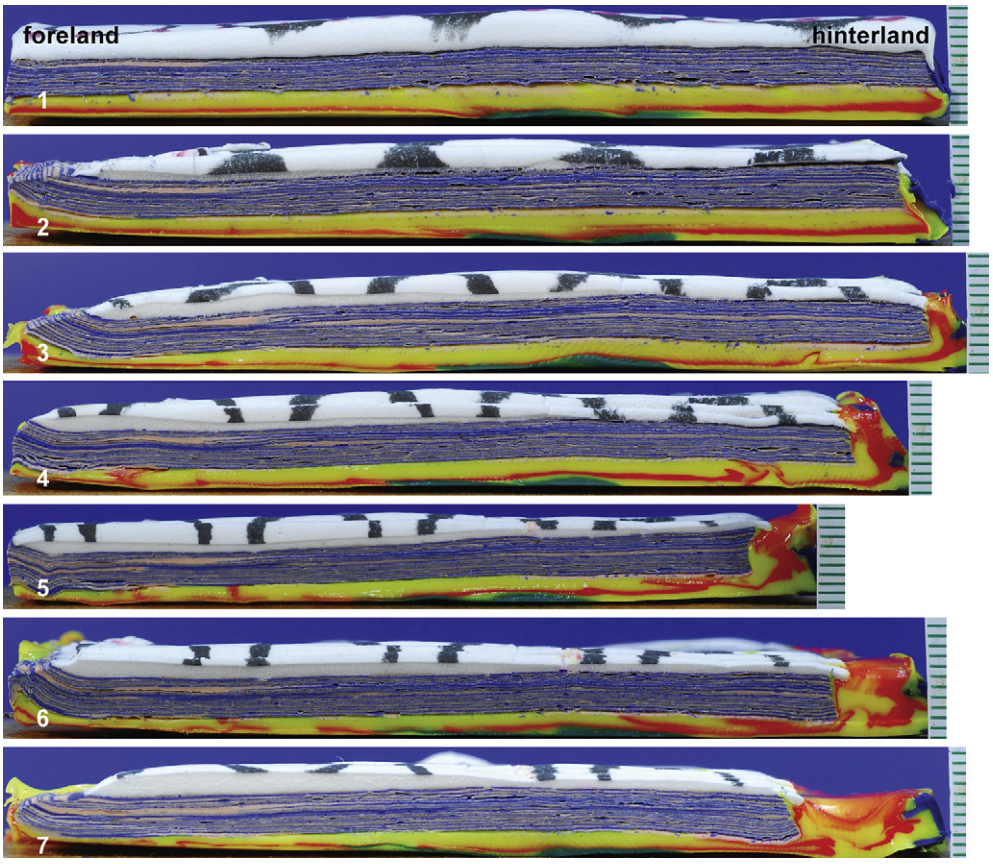

Fig. 6. Sequential photographs of Model 47. In this experiment, an erosion front cutting down to the base of the infrastructure was created during the first model run (left side) to generate a dominant foreland-directed horizontal infrastructural flow. Half the model had a steep ~60–80° and the other half a shallow ~30–45° front. Since both sides had similar behaviours, only the steep side is shown. At no time during the experiment did the superstructural package fold. The bulk of the deformation was entirely localised in the infrastructure, which underwent vertical thinning and horizontal stretching, mostly towards the erosion front, but also towards the hinterland side of the model in the later stages.

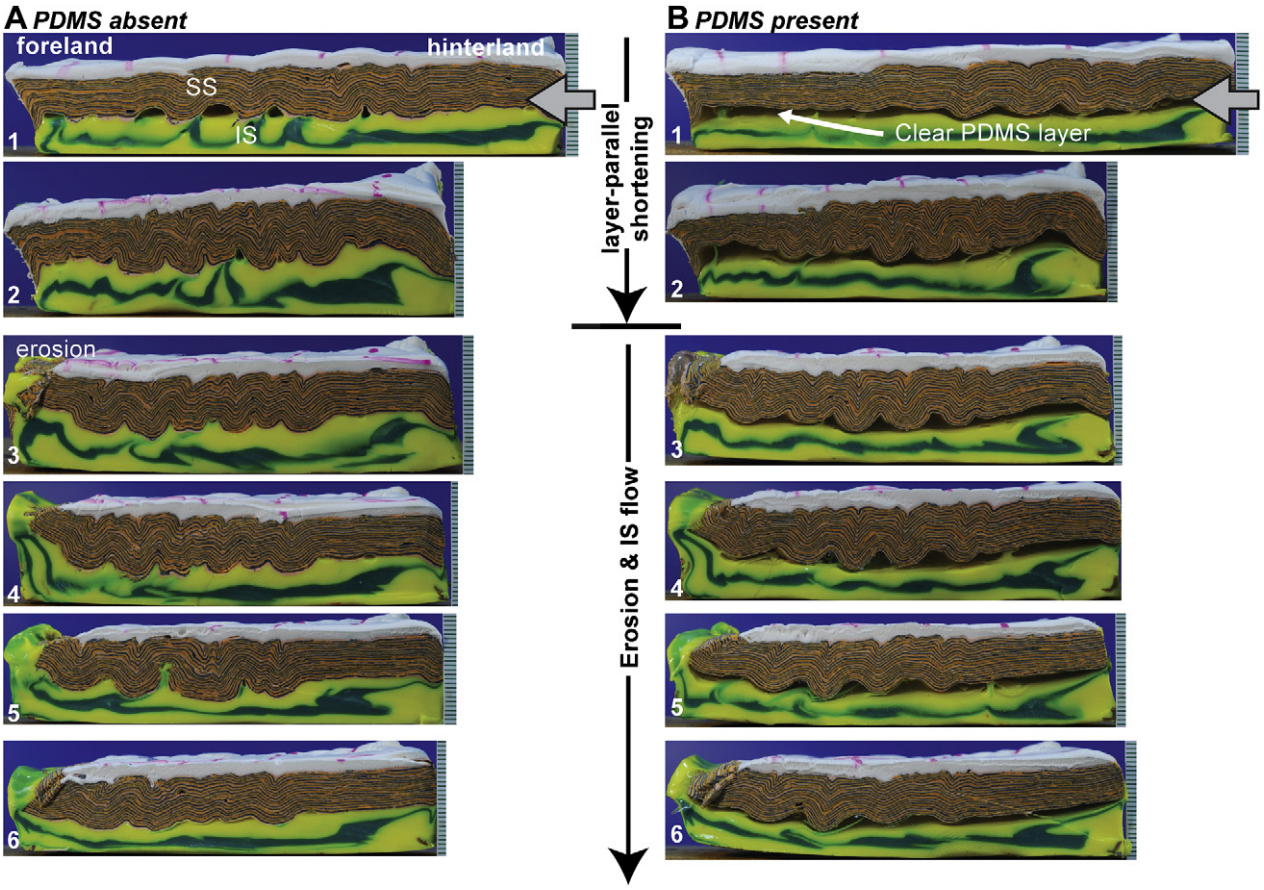

Fig. 7. Sequential photographs of Model 50 (Stages 1–6), documenting infrastructural flow induced after layer-parallel shortening. The model was divided in two: one side without polydimethylsiloxane (PDMS) at the infrastructure (IS)–superstructure (SS) contact (A), and the other side with a thin (~0.5 mm) layer of PDMS placed in the upper part of the IS to simulate the presence of leucogranites and migmatites in the upper part of the Greater Himalayan sequence (B). In Stages A1 and A2, the layer-parallel shortening is accommodated by buckle folds in the SS and by active migration of IS material in cores of SS anticlines. In B1 and B2, the anticlinal cores are filled by PDMS, with minimal vertical IS migration. In Steps 3–6 in both A and B IS lateral flow, characterised by vertical thinning and horizontal stretching, is associated with isoclinal folding near the exhumation front. The geometry of SS folds are modified by IS flow in A6, whereas there is a more efficient SS/IS decoupling visible in B5 and B6. The presence of PDMS favours more efficient decoupling between the SS and the IS, but inhibits geometrical modification of SS folds during subsequent IS lateral flow.

4.2.1. Stages 1 and 2 – deformation during the shortening phase

During the first two stages of shortening, folds in the superstructure nucleate and propagate from the hinterland towards the foreland (Fig. 7, Stages 1–2), comparable to the propagation of in-sequence thrusts predicted by critical taper (Davis et al., 1983). The initial phases of shortening produced upright open folds in the superstructure with a dominant wavelength of 8 mm. As shortening progresses, the initially open folds become progressively tighter but remain upright. The ductility of the detachment surface (presence or absence of PDMS) has no apparent effect on fold style and development in the superstructure (Fig. 7; Stages 1–2). The absence of thrusts in the model is likely due to the limitations of the materials used but may also be the product of the initial coupling between the superstructure and the underlying material that inhibits thrusting (Bonini, 2007). Fold style in the superstructure is presumably controlled by internal viscosity contrasts, depending on the rheology of the microlaminates, and coupling with the infrastructure.

When strongly coupled to the superstructure (Fig. 7a), the infrastructure developed upright to gently-inclined folds with a similar wavelength to folds in the overlying superstructure. These folds were most likely controlled by perturbations created at the base of the overlying superstructure, such as in the core of antiforms, indicating that fold style in the ductile infrastructure was most likely controlled by folds in the more competent superstructure and not *vice versa* (Fig. 7a; Stages 1–2).

When decoupled from the superstructure (Fig. 7b), the infrastructure develops broad open folds, which have a longer wavelength than those in the superstructure. These folds become progressively tighter as shortening continues. This suggests that when coupled with the infrastructure, the superstructure controls deformation in the infrastructure and when decoupled, the infrastructure deforms independently of the superstructure in the early stages of shortening (Fig. 7b; Stages 1–2).

4.2.2. Stages 3–6 – deformation during erosion

The style of deformation in the superstructure during erosion appears to be controlled by the proximity of the extruding channel and the ductility of the detachment. The most extreme change in superstructure fold geometry is found at the erosion front, proximal to the extruding infrastructure (Fig. 7a; Stages 5–6). When the ductility contrast at the interface is small and significant superstructure-infrastructure coupling exists, superstructure folds are prone to subsequent geometrical modification. When PDMS is present and the superstructure-infrastructure are effectively decoupled, modification of existing structures is slightly less apparent, but still prominent. Upright folds in the superstructure are commonly progressively modified into inclined-to-the-hinterland folds during lateral stretching of the infrastructure (Fig. 7a; Stage 6).

Erosion in the model foreland decreases the vertical lithostatic load, which creates a lateral lithostatic pressure gradient that triggers the

more ductile infrastructure to flow towards the erosion front, akin to the channel flow process (Beaumont et al., 2001, 2006; Grujic, 2006). To accommodate lateral transport, the infrastructure stretches laterally and thins vertically (e.g. Larson et al., 2010). Near-isoclinal recumbent folds either develop or are modified by rotation of existing axial planes. The infrastructure isoclinal folds often show thinned limbs (Fig. 6a, b; Stages 3–4), indicative of non-coaxial simple shear (Bons, 1993; Bons and Urai, 1996; Williams et al., 2006). These folds initiate as upright buckle folds, which axial surfaces progressively rotate towards the shear plane as the folds opening angles tighten, in a similar fashion to the evolution described by Bons (1993).

Both the coupled (without PDMS) and decoupled (with PDMS) models display 'unfolding' of the superstructure in the later stages of the models (Fig. 7; Stage 6). The exact explanation for this is unknown, but may be the product of continuous erosion in the foreland coupled with lateral gravitational collapse of the superstructure into the non-replenishing extruding infrastructure (Ramberg, 1981), or the infrastructure exerting a stretching traction on the superstructure.

4.3. *Infrastructural flow below already established superstructure folds – the influence of steepness of erosion front*

In a third model, variation in the steepness of the erosion front is used to evaluate how the foreland erosion gradient can influence

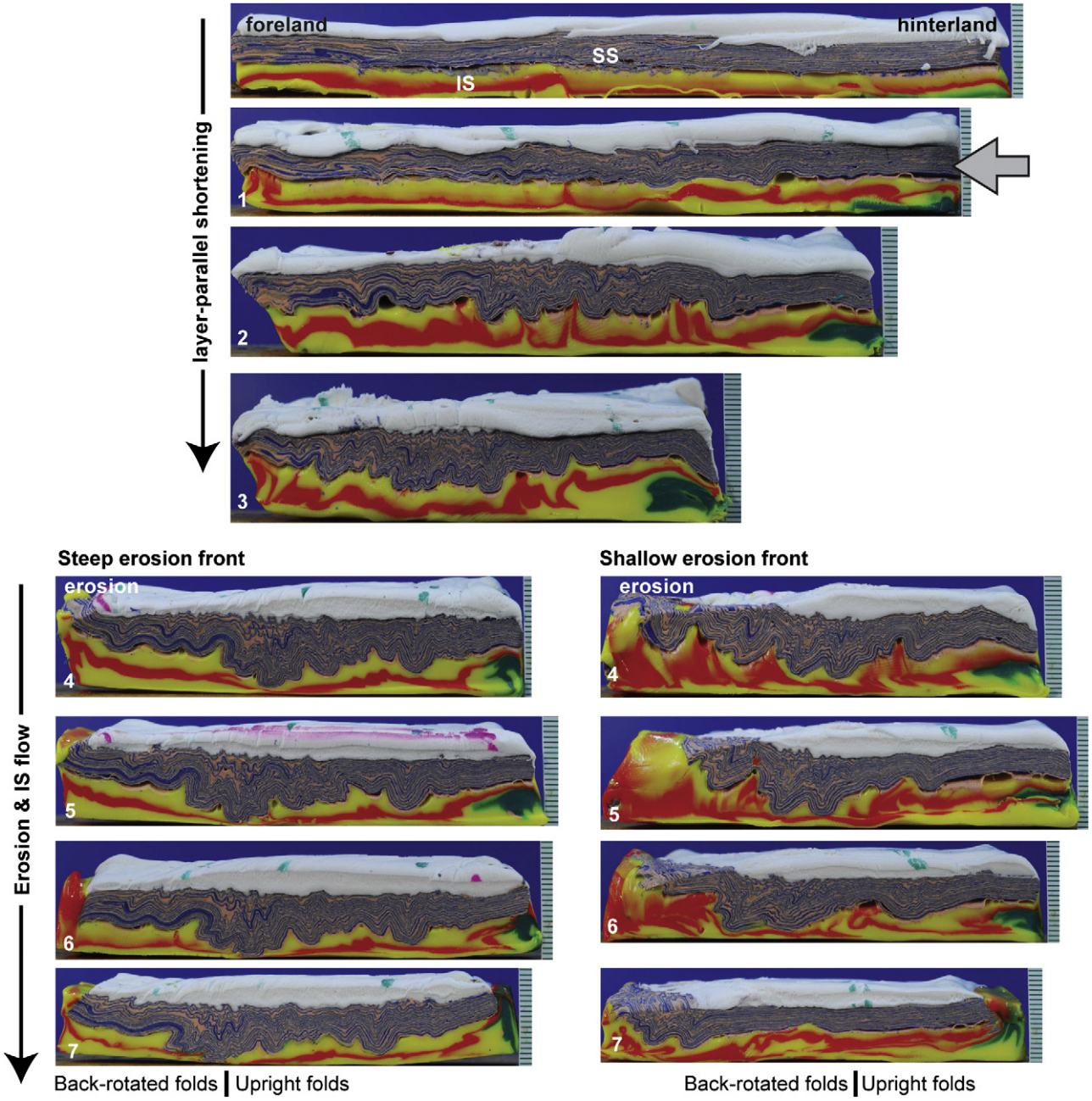

Fig. 8. Lateral flow of the infrastructure (IS) occurs during isostatic adjustments as a result of erosion in the foreland, after further shortening. The isoclinal folds in Stages 0–3 are the result of minor perturbations developed during model construction (rolling of materials). These subtle variations across the model are essential to nucleate folds comparable to those in nature (see text for discussion). During the lateral flow, folds of the superstructure (SS) progressively reorient to verge towards the hinterland. SS folds in the hinterland progressively unfold during underlying IS flow. The limit between upright and back-rotated folds is farther towards the hinterland in the presence of a shallower erosion front.

the potential for superstructural fold geometry modification. The characteristics of Model 43 are found in Table 2.

The experiment was run in seven stages (Fig. 8). The first three stages underwent 35% bulk horizontal shortening. Two different erosion fronts were then cut at the foreland end, a shallow 30° topographic front and a steep 60° front, linked by a transitional zone in the centre of the model (see Fig. 4a). The model was then run in the centrifuge for four additional stages, between which the erosion front angles were re-established (Fig. 8; Stages 4–7). The angle of the erosion front, with respect to the horizontal, has an impact on the amount of rotation of fold axial planes in the superstructure and the distance away from the erosion front where fold geometry is modified. Since erosion commenced after the shortening phase, the first three stage results are similar to Model 50, with the development of upright folds in the superstructure and slightly inclined folds in the infrastructure (Fig. 8; Stages 1–3). Modification of pre-existing structures during the erosion phase varies based on the angle of the erosion front (Fig. 8; Stages 4–7).

Similar to other models, lateral infrastructure flow occurs during lithostatic adjustments as a result of erosion in the foreland. During the lateral flow, folds of the superstructure progressively reorient to verge towards the hinterland; this is more pronounced near the steep erosion front (Fig. 8; Stages 4–7). The limit between upright and back-rotated folds is farther towards the hinterland in the presence of a shallower erosion front (~30°), compared to a steep erosion front (~60°; Fig. 8). A steep erosion front appears to favour a more localised zone of superstructure fold modification, near the foreland erosion front.

5. Discussion

5.1. Shortening sequence required for drag folding

Lateral flow of the infrastructure, partly coupled to the superstructure, has been proposed as a mechanism to nucleate folds in the lowermost superstructure (Carosi et al., 2006; Kellett and Godin, 2009). Models devoid of PDMS at the infrastructure/superstructure interface were subjected to focused erosion without shortening, which produced lateral flow of the infrastructure, but failed to nucleate folds in the superstructure (Model 47). The modelling suggests that lateral flow of the infrastructure alone cannot nucleate folds at the base of the superstructure, contrary to the proposition of Carosi et al. (2007) (Fig. 3c). The only successful way to create folds in the superstructure in the modelling is through layer-parallel shortening, as demonstrated in Models 43 and 50. The inability of infrastructural flow to generate superstructural folding may be due to a Poiseuille flow-dominated infrastructure, whereby lateral movement of the infrastructure is concentrated in the middle of the channel and the velocity decreases to zero at the channel-bounding detachment (Grujic, 2006), minimising any drag effects.

5.2. Ductility of the detachment

The superstructure anticlines formed during early shortening, in the absence of PDMS at the infrastructure interface, are cored by infrastructure material (Fig. 9a). In the presence of PDMS, however, the infrastructure remains almost planar and horizontal, and only the PDMS flows into superstructure anticlinal cores (Fig. 9b). It appears that this early geometry may control the amount of localisation and depth of the future detachment.

Without the PDMS, the detachment, which forms during the lateral infrastructure flow stage, is marked by a several-millimetre thick (equating to several km thick for the prototype) zone of decoupling in the upper part of the infrastructure, but below the infrastructure-filled anticline cores (Fig. 9c). The implication of this scenario is that part of the early infrastructure becomes incorporated in the hanging wall of the detachment. Consequently, there might not be significant metamorphic break across the decoupling fault where the active detachment is sub-horizontal.

In contrast, when PDMS is present at the superstructure-infrastructure interface (analogous to pooling of melts at the top of the Greater Himalayan sequence), the decoupling is strongly localised within the PDMS layer (Fig. 9d). Depending on the original thickness of the PDMS layer, the detachment might then isolate “pods” of PDMS in the superstructure anticlinal cores. It is conceivable in this case that cores of superstructure anticlines formed in the early stages of Himalayan orogenesis (Eocene–Oligocene) might favourably preserve migmatites, and later act as preferred location for pooling of the Miocene granitic bodies that now discontinuously appear along the strike of the orogen. It is important to note that the prototype will behave differently, because the model does not factor the cooling, therefore change of rheology, of the melts. As the superstructure is decoupling from the infrastructure, the melts (PDMS in the models) will be on a cooling (exhumation) path – hence strengthening. It follows that during exhumation of

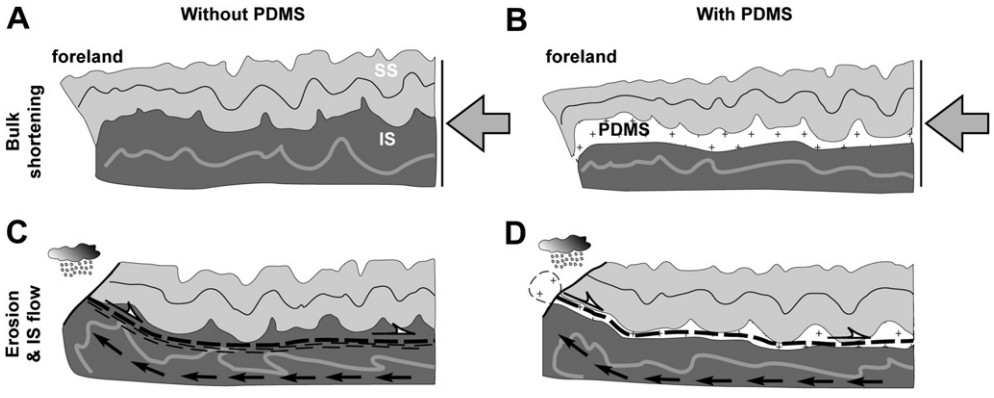

Fig. 9. Sketches depicting deformation features developed in the foreland-half of Model 50. See Fig. 7 for photographs of the experiment. (A) Without polydimethylsiloxane (PDMS) at the superstructure (SS)–infrastructure (IS) interface, initial shortening of the model develops buckle folds in the SS, while the IS material infills the SS anticlinal cores. (B) SS anticlines are cored by PDMS during early shortening, while the IS remains planar and horizontal, yet vertically thickens. (C) Once horizontal IS flow is triggered by focused foreland erosion (depicted by raining clouds), the IS–SS decoupling zone is localised in the upper part of the IS, and isolates the uppermost IS in the hanging wall of the detachment. (D) When PDMS is present, the detachment is localised within it; the entire IS is then confined to the footwall of the detachment, with only part of the PDMS isolated in the hanging wall.

the footwall, the decoupling (detachment) zone may very well step higher near the cooled melts and well-layered stratigraphy of the superstructure, where the rheological contrast and well-developed planar anisotropy would assist the localisation of the detachment.

Analogies can be made with the geology of central and eastern Nepal, whereby in regions when melt is absent, there appears to be a thick (up to 1.5 km thick) high strain zone associated with the STDS (Godin et al., 1999b; Cottle et al., 2007). When melts are present, such as in the Nar valley and the Everest massif, two clearly distinct levels of detachment are present, a ductile one immediately below (i.e. Chame detachment; Godin et al., 2006b) or above the granite (i.e. Lhotse detachment; Searle et al., 2003) and a second, younger and brittle one at the base of the unmetamorphosed Tethyan sedimentary sequence (i.e. Phu detachment; Godin et al., 2006b; Qomolangma detachment; Searle et al., 2003).

The model without PDMS may also provide insight into the structural evolution of the Haimanta Group of the Sutlej valley, NW India. The Haimanta Group is located at the Greater Himalayan sequence – Tethyan sedimentary sequence interface. It consists of interlayered psammitic and pelitic schists with minor calcareous layers (Chambers et al., 2009), similar to the Everest Series in eastern Nepal and to the Annapurna-Yellow Formation in central Nepal (as proposed by Gleeson and Godin, 2006), as well as the Chekha Group in eastern Himalaya (Grujic et al., 2002; Kellett et al., 2009). The basal part of the Haimanta Group displays minor differences in metamorphic grade with the uppermost Greater Himalayan sequence, despite being separated from it by a top-to-the-northeast shear zone. The Haimanta Group also distinguishes itself from the Greater Himalayan sequence by a distinct structural style, and a marked difference in exhumation path (Chambers et al., 2009). In this regard, the model in Fig. 9c may provide an explanation for how an early-developed portion of the infrastructure, located between the top-to-the-hinterland shear zone and the superstructure, became incorporated in the superstructure as the lower part of the infrastructure underwent later horizontal stretching flow.

5.3. Steepness and proximity of the foreland erosion front

A shallow (~30°) erosion front promotes broader extrusion of the infrastructure and a wider area of rotation of fold-axes in the superstructure into the detachment compared to a steep (~60°) erosion front (Fig. 8). This might be due to a greater component of collapse and spreading (e.g. Ramberg, 1967) in a regime with a shallower erosion angle, as suggested by unfolding of superstructure folds in the hinterland of the shallow erosion front model (see Fig. 8, Stages 6–7). A shallow model erosion front distributes the lithostatic pressure gradient over a much larger area, whereas a more abrupt gradient may be necessary to favour more efficient infrastructure flow. A steep model erosion front promotes focused, but rapid, exhumation of the infrastructure and produces a relatively minor component of collapse and spreading to fill the void created by erosion.

Fig. 10 shows a scaled comparison between the steep erosion side of Model 43 (Stage 7 of Fig. 8) and a cross section of the STDS and hanging-wall back folds, as observed in the Kali Gandaki valley of central Nepal (Godin, 2003). The two sections display striking fold geometry similarities, despite having different detachment dips. Both sections portray curved axial surface traces, progressively becoming upright (vertical) in the uppermost structural levels of the superstructure. The superstructure folds have similar fold wavelength and amplitude, and the fold geometry modification is observed only near the foreland erosion front. In both cases, the detachment is localised in the upper part of the infrastructure, and isolates part of the uppermost infrastructure (Greater

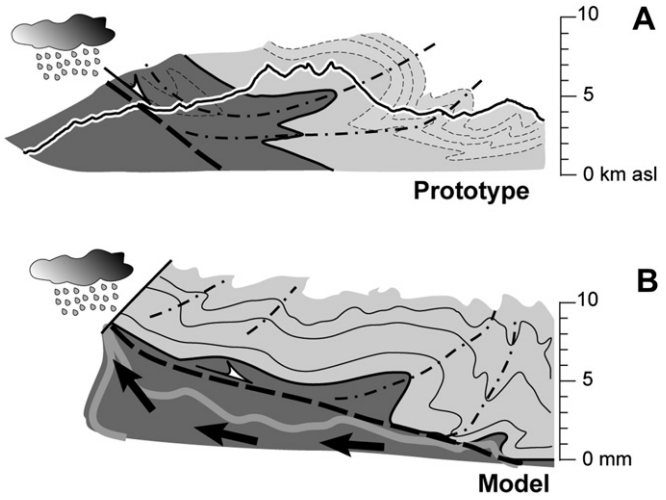

Fig. 10. Scaled comparison between (A) a geological cross section of the South Tibetan detachment and hanging-wall north-verging folds (Godin, 2003), and (B) the steep denudation side of Model 43 (see Fig. 8 for model photographs). The two sections display striking geometrical resemblance, with hanging-wall axial surface traces rotated into parallelism with the detachment surface (white line). "Raining clouds" depict focused foreland erosion. See text for discussion.

Himalayan sequence in the prototype) in anticlinal cores of the superstructure. Both prototype and model detachments also mark a clear structural boundary between the folded superstructure and the transposed (stretched and thinned) infrastructure.

The models may help resolve why hinterland-verging folds are found in central Nepal, but not elsewhere along strike. Indeed, if mid-crustal plastic flow operated along the entire strike of the orogen, it could be envisaged that such "back-folds" would have equally developed in the immediate hanging wall of the STDS in NW India (Zanskar) to Bhutan. Perhaps the answer may be a preservation one, in that the back-folds are only developed and preserved when the Tethyan sedimentary sequence folds are proximal to the foreland erosion front. In the Zanskar Himalaya of NW India, for example, the deformed Tethyan sedimentary sequence and STDS outcrop substantially north (>100 km) of the main topographic range/slope at the front of the orogenic system (Searle et al., 1997; Corfield and Searle, 2000), compared to <25 km in central Nepal.

An unresolved puzzle concerns the significant unfolding of the superstructure visible on the shallow erosion front side of Model 43 (Fig. 8; Stages 5–7). Considering that both sides of the model (steep and shallow sides) have undergone the same amount of shortening, a decrease in superstructure shortening features on the shallow side would imply either a greater amount of superstructure unfolding, or a greater amount of shortening recorded in the infrastructure, perhaps producing less horizontal stretching and greater horizontal thickening of the infrastructure. Such a geometry, if applicable to the natural prototype, would imply that P–T and strain paths for the Greater Himalayan sequence could vary dramatically as a function of the steepness of the foreland erosion front (which controls the efficiency of the infrastructural horizontal flow).

5.4. Implications for the structural evolution of the Himalayan superstructure

The modelling results support the proposition that Himalayan hinterland-verging folds preserved in the Tethyan sedimentary sequence of central Nepal are the product of early shortening of the superstructure, followed by local modification of fold geometry

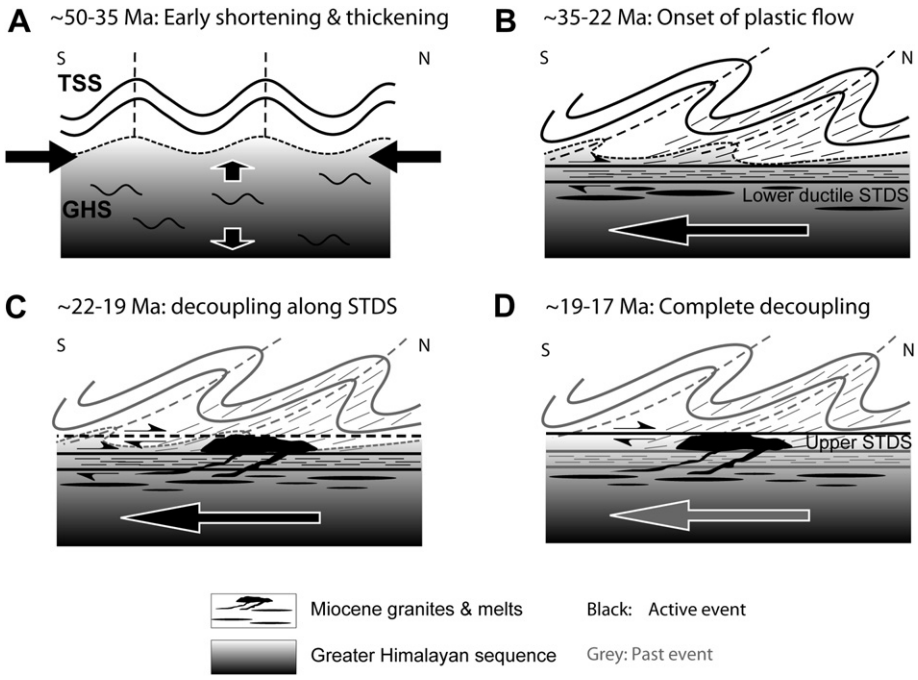

Fig. 11. (A)–(D) Tectonic evolution of the superstructure (Tethyan sedimentary sequence) in the central Nepal Himalaya, as proposed by Kellett and Godin (2009) and supported by the modelling results presented in this paper. (A) Between 50 and 35 Ma, a contractional fold belt develops in the superstructure, coupled to bulk thickening of the infrastructure. (B) From 35 to 22 Ma shortening and thickening of the superstructure continues; melt weakening in the infrastructure leads to the initiation of ductile flow of Greater Himalayan sequence towards the foreland, modifying the vergence of folds in the superstructure. (C) Between 22 and 19 Ma, melt weakening in the infrastructure intensifies and the rheological contrast between infrastructure and superstructure increases, effectively decoupling the two structural levels. Ductile extrusion of the infrastructure towards the topographic surface begins. Lateral flow of the ductile infrastructure continues at depth and anatexis leads to the emplacement of leucogranite melt bodies at the rheological boundary of the infrastructure and superstructure, further facilitating decoupling. (D) At 19–17 Ma, the rheological tip of the extruded portion of the infrastructure recedes and extruded infrastructure rocks cool. The upper, brittle component of the South Tibetan detachment system becomes activated. GHS, Greater Himalayan sequence; TSS, Tethyan sedimentary sequence, STDS, South Tibetan detachment system.

when the Greater Himalayan sequence subsequently stretched and flowed as a response to focused erosion and melt-enhanced mid-crust weakening (Fig. 3d; Kellett and Godin, 2009). The following tectonic evolution of the Tethyan sedimentary sequence in relation to the Greater Himalayan sequence is proposed (Fig. 11). The modelling results support the suggestion initially made by Brown and Nazarchuk (1993) that the northeast-verging folds preserved in the hanging wall of the STDS are a manifestation of early Himalayan superstructure shortening. According to the modelling, these folds would have initially formed upright, coupled to bulk thickening of the Greater Himalayans sequence. This early thickening event, assisted by radiogenic heat production, may have led to partial melting of the infrastructure between the onset of continental collision and the start of horizontal infrastructure flow (~50–35 Ma; Fig. 11a). From ~35–22 Ma shortening and thickening of the superstructure continued, while melt weakening in the infrastructure combined with an efficient erosion front on the Indian side of the collision instigated southward ductile flow of infrastructure rocks towards the foreland, in turn modifying the vergence of folds in the superstructure (Fig. 11b). As melt weakening in the infrastructure intensified, as evidenced by significant migmatisation and leucogranite production between ~22–19 Ma (Hodges, 2000 and references therein), the rheological contrast between infrastructure and superstructure increased. The superstructure completely decoupled from the infrastructure, while the infrastructure ductily extruded towards the topographic surface (Fig. 11c). By ~19–17 Ma, the rheological tip of the channel, behind which are rocks undergoing partial melting (i.e. Godin et al., 2006a), receded and extruded infrastructure rocks cooled. The upper, more brittle component of the STDS became activated, and consequently isolated the upper part of the Greater Himalayan sequence in its hanging wall (e.g. Haimanta-Yellow-Annapurna units; Fig. 11d).

6. Conclusions

The models demonstrate the feasibility of simulating ductile lateral flow processes using analogue materials in a high-acceleration centrifuge to reproduce infrastructure and superstructure deformation features strikingly similar to those observed in central Nepal Himalaya. Results from our analogue modelling lead to the following conclusions:

Drag from horizontal lateral flow of the infrastructure cannot alone generate shortening features in the superstructure. Superstructure folds are only successfully generated in response to bulk shortening, prior to lateral infrastructure flow. The superstructure folds are accompanied by bulk thickening of the underlying infrastructure;

Simulated focused foreland erosion produces a lateral lithostatic pressure gradient that instigates lateral flow and horizontal stretching of the infrastructure, which in turn triggers decoupling of the superstructure, and transposition of the lower structural levels of the superstructure into the detachment zone;

The presence of a weak layer (simulating pooled crustal melts) in the upper infrastructure localises a decoupling zone. Without such a weak layer, the detachment is distributed over a broader zone, and isolates part of the infrastructure in its hanging wall. This might be analogous to the situation in the Sutlej valley of NW India, where the Haimanta Group, although metamorphosed, is found in the hanging wall of the South Tibetan detachment and appears not to be affected by stretching flow characteristic of the Greater Himalayan sequence;

The geometry of the superstructure folds is only modified by infrastructure flow near the foreland erosion front. This might explain why hinterland (NE-)-verging folds have only been observed in central Nepal, where the STDS is exposed near the southern topographic front of the Himalaya;

Finally, the modelling supports the deformation sequence for the Tethyan sedimentary sequence, as proposed by Kellett and Godin (2009), whereby the Himalayan hinterland folds observed in central Nepal are the product of early crustal shortening forming upright folds, modified during Greater Himalayan sequence horizontal stretching flow during the Miocene.

The models presented in this paper highlight the frequent observation that the superstructure and infrastructure of many orogens may portray contrasting fold styles suggesting different tectonic histories, but which can develop coevally. The geometry and vergence of superstructure folds in an orogen may therefore not represent their initial configuration and may not reflect the sense of bulk tectonic transport.

Acknowledgements

Acknowledgement is made to the Donors of the American Chemical Society Petroleum Research Fund for support of centrifuge modelling research at INRS-ETE and to NSERC for Discovery grants to L. Harris and L. Godin. Modelling was undertaken at INRS-ETE by C. Yakymchuk, recipient of an NSERC USRA Summer Research Scholarship. The laboratory for physical, numerical, and geophysical simulations at INRS-ETE was funded by CFI and MELS-Q grants to L. Harris with contributions from INRS-ETE, Applied Geodynamics Laboratory of the Bureau of Economic Geology (University of Texas at Austin), Sun Microsystems, Seismic Microtechnology, and Norsar. D. Kellett, A. Cruden, K. Stübner, and an anonymous reviewer provided insightful reviews that helped clarify the manuscript. Their constructive comments, along with those from Editor Dazhi Jiang, are gratefully acknowledged.

References

Aikman, A.B., Harrison, T.M., Lin, D., 2008. Evidence for early (44 Ma) Himalayan crustal thickening, Tethyan Himalaya, southeastern Tibet. Earth and Planetary Science Letters 274, 14–23.

Alsop, G.I., Holdsworth, R.E., McCaffrey, K.J.W., 2007. Scale invariant sheath folds in salt, sediments and shear zones. Journal of Structural Geology 29, 1585–1604.

Beaumont, C., Jamieson, R.A., Nguyen, M.H., Lee, B., 2001. Himalayan tectonics explained by extrusion of a low-viscosity crustal channel coupled to focused surface denudation. Nature 414, 738–742.

Beaumont, C., Nguyen, M.H., Jamieson, R.A., Ellis, S., 2006. Crustal flow modes in large hot orogens. In: Law, R.D., Searle, M.P., Godin, L. (Eds.), Channel Flow, Ductile Extrusion and Exhumation in Continental Collision Zones. Geological Society, London, Special Publication 268, pp. 91–145.

Bird, P., 1991. Lateral extrusion of lower crust from under high topography, in the isostatic limit. Journal of Geophysical Research 96, 10275–10286.

Bonini, M., 2007. Deformation patterns and structural vergence in brittle-ductile thrust wedges: an additional analogue modeling perspective. Journal of Structural Geology 29, 141–158.

Bons, P.D., 1993. Experimental deformation of polyphase rock analogues. Geologica Ultraiectina: Mededelingen van de Faculteit Aardwetenschappen der Universiteit Utrecht 110, 1–207.

Bons, P.D., Urai, J.L., 1996. An apparatus to experimentally model the dynamics of ductile shear zones. Tectonophysics 256, 145–164.

Bordet, P., Colchen, M., Krummenacher, D., Le Fort, P., Mouterde, R., Remy, M., 1971. Recherches géologiques dans l'Himalaya du Népal: région de la Thakhola. Centre National de la Recherche Scientifique, Paris, France, 279 pp.

Brown, R.L., Nazarchuk, J.H., 1993. Annapurna detachment fault in the Greater Himalaya of central Nepal. In: Treloar, P.J., Searle, M.P. (Eds.), Himalayan Tectonics. Geological Society, London, Special Publication 74, pp. 461–773.

Brun, J.P., Merle, O., 1988. Experiments on folding in spreading-gliding nappes. Tectonophysics 145, 129–139.

Burbank, D.W., Leland, J., Fielding, E., Anderson, R.S., Brozovic, N., Reid, M.R., Duncan, C., 1996. Bedrock incision, rock uplift and threshold hillslopes in the northwestern Himalaya. Nature 379, 505–510.

Burchfiel, B.C., Royden, L.H., 1985. North-south extension within the convergent Himalayan region. Geology 13, 679–682.

Burchfiel, B.C., Chen, Z., Hodges, K.V., Liu, Y., Royden, L.H., Deng, C., Xu, J., 1992. The South Tibetan detachment system, Himalaya orogen: extension contemporaneous with and parallel to shortening in a collisional mountain belt. Geological Society of America, Special Paper 269, 1–41.

Burg, J.-P., Chen, G.M., 1984. Tectonics and structural zonation of southern Tibet, China. Nature 311, 219–223.

Carosi, R., Montomoli, C., Rubatto, D., Visonà, D., 2006. Normal-sense shear zones in the core of the Higher Himalayan Crystallines (Bhutan Himalaya): evidence for extrusion? In: Law, R.D., Searle, M.P., Godin, L. (Eds.), Channel Flow, Ductile Extrusion and Exhumation in Continental Collision Zones Geological Society, London, Special Publication 268, pp. 425–444.

Carosi, R., Montomoli, C., Visonà, D., 2007. A structural transect in the Lower Dolpo: insights on the tectonic evolution of Western Nepal. Journal of Asian Earth Sciences 29, 407–423.

Chambers, J., Caddick, M., Argles, T., Horstwood, M., Sherlock, S., Harris, N., Parrish, R., Ahmad, T., 2009. Empirical constraints on extrusion mechanisms from the upper margin of an exhumed high-grade orogenic core, Sutlej valley, NW India. Tectonophysics 477, 77–92.

Clark, M.K., Royden, L.H., 2000. Topographic ooze: building the eastern margin of Tibet by lower crustal flow. Geology 28, 703–706.

Colchen, M., Le Fort, P., Pêcher, A., 1981. Geological map of Annapurnas–Manaslu–Ganesh Himalaya of Nepal. In: Gupta, H.K., Delany, F.M. (Eds.), Zagros-Hindu Kush-Himalaya Geodynamic Evolution. American Geophysical Union, Washington, DC Scale 1:200,000.

Corfield, R.I., Searle, M.P., 2000. Crustal shortening estimates across the north Indian continental margin, Ladakh, NW India. In: Asif Khan, M., Treloar, P.J., Searle, M.P., Qasim Jan, M. (Eds.), Tectonics of the Nanga Parbat Syntaxis and the Western Himalayas. Geological Society, London, Special Publication 170, pp. 395–410.

Corti, G., 2004. Centrifuge modelling of the influence of crustal fabrics on the development of transfer zones: insights into the mechanics of continental rifting architecture. Tectonophysics 384, 191–208.

Cottle, J.M., Jessup, M.J., Newell, D.L., Searle, M.P., Law, R.D., Horstwood, M.S.A., 2007. Structural insights into the early stages of exhumation along an orogen-scale detachment: the South Tibetan Detachment System, Dzakaa Chu section, Eastern Himalaya. Journal of Structural Geology 29, 1781–1797.

Culshaw, N.G., Beaumont, C., Jamieson, R.A., 2006. The orogenic superstructure-infrastructure concept: revisited, quantified, and revived. Geology 34, 733–736.

Daniel, C.G., Hollister, L.S., Parrish, R.R., Grujic, D., 2003. Exhumation of the Main Central thrust from lower crustal depths, eastern Bhutan Himalaya. Journal of Metamorphic Geology 21, 317–334.

Denèle, Y., Olivier, P., Gleizes, G., Barbey, P., 2009. Decoupling between the middle and upper crust during transpression-related lateral flow: Variscan evolution of the Aston gneiss dome (Pyrenees, France). Tectonophysics 477, 244–261.

Davis, D., Suppe, J., Dahlen, F.A., 1983. Mechanics of fold-and-thrust belts and accretionary wedges. Journal of Geophysical Research 88, 1153–1172.

Dixon, J.M., Tirrul, R., 1991. Centrifuge modelling of fold-thrust structures in a tripartite stratigraphic succession. Journal of Structural Geology 13, 3–20.

Dixon, J.M., Summers, J.M., 1985. Recent developments in centrifuge modelling of tectonic processes: equipment, model construction techniques and rheology of model materials. Journal of Structural Geology 7, 83–102.

Gabet, E., Pratt-Sitaula, B.A., Burbank, D.W., 2004. Climatic controls on hillslope angle and relief in the Himalaya. Geology 32, 629–632.

Garzanti, E., 1999. Stratigraphy and sedimentary history of the Nepal Tethys Himalaya passive margin. Journal of Asian Earth Sciences 17, 805–827.

Gleeson, T., Godin, L., 2006. The Chako antiform: A folded segment of the Greater Himalayan sequence, Nar valley, Central Nepal Himalayal. Journal of Asian Earth Sciences 27, 717–734.

Glombick, P., Thompson, R.I., Erdmer, P., Daughtry, K.L., 2006. A reappraisal of the tectonic significance of early Tertiary low-angle shear zones exposed in the Vernon map area (82 L), Shuswap metamorphic complex, southeastern Canadian Cordillera. Canadian Journal of Earth Sciences 43, 245–268.

Godin, L., 2003. Structural evolution of the Tethyan sedimentary sequence, central Nepal Himalaya. Journal of Asian Earth Sciences 22, 307–328.

Godin, L., Brown, R.L., Hanmer, S., Parrish, R., 1999a. Backfolds in the core of the Himalayan orogen: an alternative interpretation. Geology 27, 151–154.

Godin, L., Brown, R.L., Hanmer, S., 1999b. High strain zone in the hanging wall of the Annapurna detachment, central Nepal Himalaya. In: Macfarlane, A.M., Sorkhabi, R., Quade, J. (Eds.), Himalaya and Tibet: Mountain Roots to Mountain Tops. Geological Society of America, Special Paper 328, pp. 199–210.

Godin, L., Parrish, R.R., Brown, R.L., Hodges, K., 2001. Crustal thickening leading to exhumation of the metamorphic core of the central Nepal Himalaya: insight from U–Pb geochronology and $^{40}Ar/^{39}Ar$ thermochronology. Tectonics 20, 729–747.

Godin, L., Grujic, D., Law, R.D., Searle, M.P., 2006a. Channel flow, extrusion, and exhumation in continental collision zones: an introduction. In: Law, R.D., Searle, M.P., Godin, L. (Eds.), Channel Flow, Ductile Extrusion and Exhumation in Continental Collision Zones. Geological Society, London, Special Publication 268, pp. 1–23.

Godin, L., Gleeson, T., Searle, M.P., Parrish, R.R., Ullrich, T.D., 2006b. Locking of southward extrusion in favor of rapid crustal-scale buckling of the Greater Himalayan sequence, Nar Valley, central Nepal. In: Law, R.D., Searle, M.P.,

Godin, L. (Eds.), Channel Flow, Ductile Extrusion and Exhumation in Continental Collision Zones. Geological Society, London, Special Publication 268, pp. 269–292.
Gradstein, F.M., von Rad, U., Gibling, M.R., Jansa, L.F., Kaminski, M.A., Kristiansen, I.-L., Ogg, J.G., Rohl, U., Sarti, M., Thorow, J.W., Westermann, G.E.G., Wiedmann, J., 1992. The Mesozoic continental margin of central Nepal. Geologisches Jahrbuch 77.
Grasemann, B., Fritz, H., Vannay, J.-C., 1999. Quantitative kinematic flow analysis from the Main Central thrust zone (NW-Himalaya, India): implications for a decelerating strain path and the extrusion of orogenic wedges. Journal of Structural Geology 21, 837–853.
Grujic, D., 2006. Channel flow and continental collision tectonics: an overview. In: Law, R.D., Searle, M.P., Godin, L. (Eds.), Channel Flow, Ductile Extrusion and Exhumation in Continental Collision Zones. Geological Society, London, Special Publication 268, pp. 25–37.
Grujic, D., Casey, M., Davidson, C., Hollister, L.S., Kündic, R., Pavlis, T., Schmid, S., 1996. Ductile extension of the Higher Himalayan Crystalline in Bhutan: evidence from quartz microfabrics. Tectonophysics 260, 21–43.
Grujic, D., Hollister, L.S., Parrish, R.R., 2002. Himalayan metamorphic sequence as an orogenic channel: insight from Bhutan. Earth and Planetary Science Letters 198, 177–191.
ten Grotenhuis, S.M., Piazolo, S., Pakula, T., Passchier, C.W., Bons, P.D., 2002. Are polymers suitable rock analogs? Tectonophysics 350, 35–47.
Guillot, S., Pêcher, A., Rochette, P., Le Fort, P., 1993. The emplacement of the Manaslu granite of central Nepal: field and magnetic susceptibility constraints. In: Treloar, P.J., Searle, M.P. (Eds.), Himalayan Tectonics. Geological Society, London, Special Publication 74, pp. 413–428.
Harris, L.B., Koyi, H.A., 2003. Centrifuge modelling of folding in high-grade rocks during rifting. Journal of Structural Geology 25, 291–305.
Hodges, K.V., 2000. Tectonics of the Himalaya and southern Tibet from two perspectives. Geological Society of America Bulletin 112, 324–350.
Hodges, K.V., Parrish, R.R., Housh, T.B., Lux, D.R., Burchfiel, B.C., Royden, L.H., Chen, Z., 1992. Simultaneous Miocene extension and shortening in the Himalayan orogen. Science 258, 1466–1470.
Hodges, K.V., Parrish, R.R., Searle, M.P., 1996. Tectonic evolution of the central Annapurna Range, Nepalese Himalayas. Tectonics 15, 1264–1291.
Hollister, L.S., Grijuc, D., 2006. Pulsed channel flow in Bhutan. In: Law, R.D., Searle, M.P., Godin, L. (Eds.), Channel Flow, Ductile Extrusion and Exhumation in Continental Collision Zones. Geological Society, London, Special Publication 268, pp. 415–423.
Hubbard, M.S., Harrison, T.M., 1989. $^{40}Ar/^{39}Ar$ age constraints on deformation and metamorphism in the Main Central Thrust Zone and Tibetan Slab, eastern Nepal Himalaya. Tectonics 8, 865–880.
Hubbert, M.K., 1937. Theory of scale models as applied to the study of geologic structures. Bulletin of the Geological Society of America 48, 1459–1520.
Jamieson, R.A., Beaumont, C., Hamilton, J., Fullsack, P., 1998. Tectonic assembly of inverted metamorphic sequences. Geology 24, 839–842.
Jamieson, R.A., Beaumont, C., Medvedev, S., Nguyen, M.H., 2004. Crustal channel flows: 2. Numerical models with implications for metamorphism in the Himalayan-Tibetan orogen. Journal of Geophysical Research 109. doi:10.1029/2003JB002811.
Jessup, M.J., Law, R.D., Searle, M.P., Hubbard, M.S., 2006. Structural evolution and vorticity of flow during extrusion and exhumation of the Greater Himalayan Slab, Mount Everest Massif, Tibet/Nepal: implications for orogen-scale flow partitioning. In: Law, R.D., Searle, M.P., Godin, L. (Eds.), Channel Flow, Ductile Extrusion and Exhumation in Continental Collision Zones. Geological Society, London, Special Publication 268, pp. 379–413.
Johns, M.K., Mosher, S., 1996. Physical models of regional fold superposition: the role of competence contrast. Journal of Structural Geology 18, 475–492.
Kellett, D.A.-M., Godin, L., 2009. Pre-Miocene deformation of the Himalayan superstructure, central Nepal. Journal of the Geological Society, London 166, 261–274.
Kellett, D.A.-M., Grujic, D., Erdmann, S., 2009. Miocene structural reorganization of the South Tibetan detachment, eastern Himalaya: implications for continental collision. Lithosphere 1, 259–281.
Koyi, H., 1991. Gravity overturns, extension, and basement fault reactivation. Journal of Petroleum Geology 14, 117–142.
Koyi, H.A., Skelton, A., 2001. Centrifuge modelling of the evolution of low-angle detachment faults from high-angle normal faults. Journal of Structural Geology 23, 1179–1185.
Larson, K.P., Godin, L., 2009. Kinematics of the Greater Himalayan sequence, Dhaulagiri Himal: implications for the structural framework of central Nepal. Journal of the Geological Society, London 166, 25–43.
Larson, K.P., Godin, L., Price, R.A., 2010. Relationships between displacement and distortion in orogens: linking the Himalayan foreland and hinterland of central Nepal. Geological Society of America Bulletin 122, 1116–1134.
Law, R.D., Searle, M.P., Simpson, R.L., 2004. Strain, deformation temperatures and vorticity of flow at the top of the Greater Himalayan slab, Everest massif, Tibet. Journal of the Geological Society, London 161, 305–320.
Mancktelow, N.S., 1999. Finite-element modelling of single-layer folding in elasto-viscous materials: the effect of initial perturbation geometry. Journal of Structural Geology 21, 161–177.
Mattauer, M., 1975. Sur le mécanisme de formation de la schistosité dans l'Himalaya. Earth and Planetary Science Letters 28, 144–154.
Mecklenburgh, J., Rutter, E.H., 2003. On the rheology of partially molten synthetic granite. Journal of Structural Geology 25, 1575–1585.
Murphy, D.C., 1987. Suprastructurel/infrastructure transition, east-central Cariboo Mountains, British Columbia: geometry, kinematics and tectonic implications. Journal of Structural Geology 9, 13–29.
Poulin, J., 2006. De la médecine à la géologie - visualisation des modèles physiques par tomodensitométrie. M.Sc. Thesis, INRS-ETE, Québec, http://ete.inrs.ca/pub/theses/T000478.pdf and http://ete.inrs.ca/pub/theses/T000478.zip [accessed April 2010].
Raimondo, T., Collins, A.S., Hand, M., Walker-Hallam, A., Smithies, R.H., Evins, P.M., Howard, H.M., 2009. Ediacaran intracontinental channel flow. Geology 37, 291–294.
Ramberg, H., 1967. Gravity, Deformation and The Earth's Crust. Academic Press, London.
Ramberg, H., 1981. Gravity, deformation and the Earth's crust. In: Theory, Experiments and Geological Applications, second ed. Academic Press, London.
Robinson, D.M., DeCelles, P.G., Copeland, P., 2006. Tectonic evolution of the Himalayan thrust belt in western Nepal: implications for channel flow models. Geological Society of America Bulletin 118, 865–885.
Rosenberg, C.L., Handy, M.R., 2005. Experimental deformation of partially melted granite revisited: implications for the continental crust. Journal of Metamorphic Geology 23, 19–28.
Royden, L.H., Burchfiel, B.C., King, R.W., Chen, Z., Shen, F., Liu, Y., 1997. Surface deformation and lower crustal flow in eastern Tibet. Science 276, 788–790.
Searle, M.P., Rex, A.J., 1989. Thermal model for the Zanskar Himalaya. Journal of Metamorphic Geology 7, 127–134.
Searle, M.P., Godin, L., 2003. The South Tibetan detachment system and the Manaslu leucogranite: a structural reinterpretation and restoration of the Annapurna – Manaslu Himalaya, Nepal. Journal of Geology 111, 505–524.
Searle, M.P., Szulc, A.G., 2005. Channel flow and ductile extrusion of the high Himalayan slab-the Kangchenjunga–Darjeeling profile, Sikkim Himalaya. Journal of Asian Earth Sciences 25, 173–185.
Searle, M.P., Corfield, R.I., Stephenson, B.J., McCarron, J., 1997. Structure of the North Indian continental magin in the Ladakh – Zanskar Himalayas: implications for the timing of ophiolite obduction, India – Asia collision and deformation events in the Himalaya. Geological Magazine 134, 297–316.
Searle, M.P., Simpson, R.L., Law, R.D., Parrish, R.R., Waters, D.J., 2003. The structural geometry, metamorphic and magmatic evolution of the Everest massif, High Himalaya of Nepal-South Tibet. Journal of the Geological Society, London 160, 345–366.
Searle, M.P., Warren, C.J., Waters, C.J., Parrish, R.R., 2004. Structural evolution, metamorphism and restoration of the Arabian continental margin, Saih Hatat region, Oman Mountains. Journal of Structural Geology 26, 451–473.
Searle, M.P., Law, R.D., Godin, L., Larson, K.P., Streule, M.J., Cottle, J.M., Jessup, M.J., 2008. Defining the Himalayan Main Central thrust in Nepal. Journal of the Geological Society of London 165, 523–534.
Vannay, J.-C., Hodges, K.V., 1996. Tectonometamorphic evolution of the Himalayan metamorphic core between the Annapurna and Dhaulagiri, central Nepal. Journal of Metamorphic Geology 14, 635–656.
Wegmann, C.E., 1935. Zur Deutung der Migmatite. Geologische Rundschau 26, 205–350.
Weijermars, R., 1986. Flow behaviour and physical chemistry of bouncing putties and related polymers in view of tectonic laboratory applications. Tectonophysics 124, 325–358.
Williams, P.F., Jiang, D., 2001. The role of initial perturbations in the development of folds in a rock-analogue. Journal of Structural Geology 23, 845–856.
Williams, P.F., Jiang, D., 2005. An investigation of lower crustal deformation: evidence for channel flow and its implications for tectonics and structural studies. Journal of Structural Geology 27, 1486–1504.
Williams, P.F., Jiang, D., Lin, S., 2006. Interpretation of deformation fabrics of infrastructure zone rocks in the context of channel flow and other tectonic models. In: Law, R.D., Searle, M.P., Godin, L. (Eds.), Channel Flow, Ductile Extrusion and Exhumation in Continental Collision Zones. Geological Society, London, Special Publication 268, pp. 221–235.
Yin, A., Harrison, T.M., 2000. Geologic evolution of the Himalayan-Tibetan orogen. Annual Reviews in Earth and Planetary Science 28, 211–280.